ADVANCED FUNCTIONAL MATERIALS

FULL PAPER

DOI: 10.1002/adfm.200700039

Covalent Functionalization of Carbon Nanohorns with Porphyrins: Nanohybrid Formation and Photoinduced Electron and Energy Transfer**

By *Georgia Pagona*, *Atula S. D. Sandanayaka*, *Yasuyuki Araki*, *Jing Fan*, *Nikos Tagmatarchis*,* *Georgios Charalambidis*, *Athanassios G. Coutsolelos*,* *Bernard Boitrel*, *Masako Yudasaka*, *Sumio Iijima*, and *Osamu Ito**

The covalent attachment of carbon nanohorns (CNHs) to α-5-(2-aminophenyl)-α-15-(2-nitrophenyl)-10,20-bis(2,4,6-trimethylphenyl)-porphyrin (H_2P) via an amide bond is accomplished. The resulting CNH–H_2P nanohybrids form a stable inklike solution. High-resolution transmission electron microscopy (HRTEM) images demonstrate that the original dahlia-flowerlike superstructure of the CNHs is preserved in the CNH–H_2P nanohybrids. Steady-state and time-resolved fluorescence studies show efficient quenching of the excited singlet state of H_2P, suggesting that both electron and energy transfer occur from the singlet excited state of H_2P to CNHs, depending on the polarity of the solvent. In the case of electron transfer, photoexcitation of H_2P results in the reduction of the nanohorns and the simultaneous oxidation of the porphyrin unit. The formation of a charge-separated state, $CNH^{\bullet-}$–$H_2P^{\bullet+}$, has been corroborated with the help of an electron mediator, hexyl-viologen dication (HV^{2+}), in polar solvents. Moreover, the charge-separated $CNH^{\bullet-}$–$H_2P^{\bullet+}$ states have been identified by transient absorption spectroscopy.

1. Introduction

Carbon nanohorns (CNHs) represent promising alternatives to carbon nanotubes, and have started emerging as interesting nanometer-sized building blocks for the construction of novel materials with potential applications in nanotechnology.[1] Typically, CNHs are produced by the CO_2 laser ablation of pure graphite under an argon atmosphere in the absence of any metallic additives.[2] The characteristic features of CNHs include the conical end termination on one side of their tubular structure and their aggregation in spherical assemblies of 50–100 nm dahlia-flower-like superstructures. Additionally, the CNHs are characterized by a high surface area, excellent porosity, and considerable internal nanospace, which make them promising candidates for use in future practical clean-energy technologies and drug-delivery applications.[3,4]

The rough surface structure of the CNH aggregates prevents the increase of the aggregate–aggregate contact area, resulting in weak Van der Waals interactions between the structures, and thus enabling better dispersion of the CNHs in selected organic solvents (such as dimethylformamide (DMF) and toluene) as compared to carbon nanotubes, which tend to be rather difficult to disperse. Moreover, issues related to the insolubility of pristine CNHs have been recently been resolved to a great extent with the help of chemical functionalization procedures involving the covalent attachment of organic species either to the sidewalls or to the open conical ends of the nanohorns.[5–7] In addition, the non-covalent π–π interactions of CNHs with pyrenes offers another complementary approach towards enhancing the solubilization of the nanohorns.[8]

[*] Dr. N. Tagmatarchis, G. Pagona
Theoretical and Physical Chemistry Institute
National Hellenic Research Foundation
48 Vass. Constantinou Ave., Athens 116 35 (Greece)
E-mail: tagmatar@eie.gr
Prof. A. G. Coutsolelos, G. Charalambidis
Chemistry Department, Laboratory of BioInorganic Chemistry
University of Crete
PO Box 2208, 710 03 Heraklion, Crete (Greece)
E-mail: coutsole@chemistry.uoc.gr
Prof. O. Ito, A. S. D. Sandanayaka, Dr. Y. Araki
Institute of Multidisciplinary Research for Advanced Materials
Tohoku University
Katahira, Aoba-ku, Sendai, 980-8577 (Japan)
E-mail: ito@tagen.tohoku.ac.jp
J. Fan, Dr. M. Yudasaka, Prof. S. Iijima
Fundamental and Environmental Research Laboratories
NEC Corporation and SORST-JST
34 Miyukigaoka, Tsukuba, Ibaraki 305850 (Japan)
Prof. B. Boitrel
Institut de Chimie, UMR CNRS 6509
Organométalliques et Catalyse, Chimie et Electrochimie Moléculaire
Université de Rennes1
35042 Rennes Cedex (France)

[**] This work, conducted as part of the award "Functionalization of Carbon Nanotubes Encapsulating Novel Carbon-Based Nanostructured Materials" under the European Heads of Research Councils and European Science Foundation European Young Investigator (EURYI) Awards Scheme, was supported by funds from the Participating Organizations of EURYI and the EC Sixth Framework Programme. The present work was also supported by Grants-in-Aid on Scientific Research on Priority Areas (417) from the Ministry of Education, Culture, Sports, Science, and Technology of Japan. Supporting Information is available online from Wiley InterScience or from the author.

The ability of the CNHs to accept electrons and the ability of the electrons to readily diffuse along the main conical axis with negligible energy loss have inspired the synthesis of the first examples of donor–acceptor nanosystems utilizing CNHs and covalently attached pyrenes; the pyrenes are attached either at the sidewalls or at the conical tips.[5a,6] In addition, we have recently demonstrated the immobilization of a water-soluble tetracationic porphyrin H_2P^{4+} onto CNHs. Upon illumination with light, electron-transfer processes are observed within the resulting nanohybrid,[9] which is similar to the phenomena observed for carbon-nanotube/porphyrin systems linked together by supramolecular association and/or electrostatic interactions.[10] The novel and intriguing photophysical properties of porphyrins have inspired us to explore, for the first time, their utility when covalently attached to CNHs.

The aim of the study described herein is three-fold: i) to provide evidence for the covalent attachment of strong photoinduced electron donors such as porphyrins to CNHs, ii) to perform a detailed photophysical study and shed light on the dynamics of the resulting hybrid nanosystems, and iii) to compare the obtained data with the reported results for other elongated carbon nanostructures such as carbon nanotubes.[11]

2. Results and Discussion

The porphyrin utilized in this study, α-5-(2-aminophenyl)-α-15-(2-nitrophenyl)-10,20-bis(2,4,6-trimethyl-phenyl)-porphyrin (abbreviated as H_2P), is obtained via the [2 + 2] MacDonald cycloaddition of mesityl aldehyde to pyrrole, followed by cyclization of the formed dipyrrole with *ortho*-nitrobenzaldehyde. Selective reduction of only one of the two nitro groups of the intermediate, α-5,15-bis(2-nitrophenyl)-10,20-bis(2,4,6-trimethyl-phenyl)-porphyrin, gives rise to a mixture of α,α- and α,β-atropisomers, which are separated and isolated in pure form by column chromatography.[12] Eventually, the structure of H_2P is confirmed by a variety of complementary spectroscopic tools, including ^1H and ^{13}C NMR spectroscopy (Supporting Information, Figs. S1–S3). Although a nitro group is present at the ortho-position of one of the meso-attached phenyl rings, the electron donating ability of H_2P with two mesityl groups is still retained.

The pristine CNHs are heated in the presence of oxygen (580 °C, 10 min.) in order to remove the conical tips and to introduce carboxylic acid functionalities. Under anaerobic and dry conditions, the treatment of activated CNHs with H_2P (detailed experimental procedures are provided in the Supporting Information) results in the covalent coupling of the free amino functional group of H_2P molecules with acyl chloride moieties on the activated CNHs. The hybrid material, denoted as CNH–H_2P, is obtained as black solid by filtration of the reaction mixture through a 0.2 μm poly(tetrafluoroethylene) (PTFE) filter, followed by sufficient washing with organic solvents to remove unbound free H_2P. The CNH–H_2P nanohybrids (Fig. 1) have been found to be soluble in dichloromethane, tetrahydrofuran (THF), and toluene for several weeks, forming stable black solutions. No significant precipitation is observed from the solubilized material, providing strong evidence for the good stability of the hybrid material.

High-resolution transmission electron microscopy (HRTEM) and dynamic light scattering (DLS) measurements have been used to probe the morphological characteristics and particle size distribution of the CNH–H_2P nanohybrids, respectively. In this context, HRTEM analysis reveals that the spherical superstructure of the CNHs is predominantly retained, as shown in Figure 2a. This demonstrates that the covalent attachment of a large pigment such as the current porphyrin does not

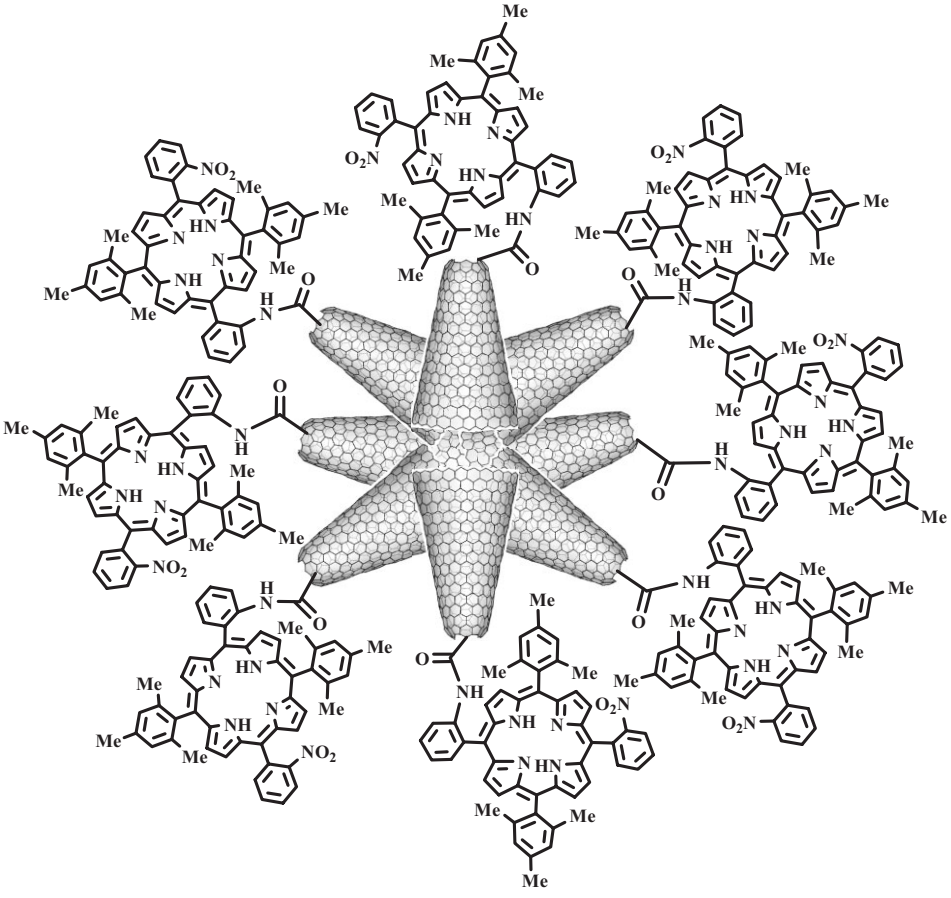

Figure 1. Schematic depiction of the structure of CNH–H_2P nanohybrids. The other oxygenated species (i.e., hydroxyls, carbonyls, ethers, etc) introduced during the oxidation of CNHs are not shown for simplicity.

ADVANCED FUNCTIONAL MATERIALS

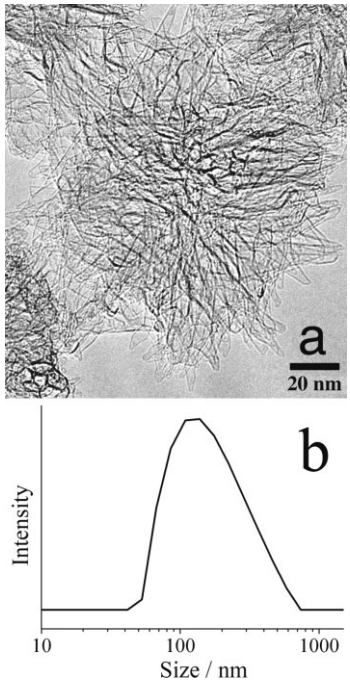

Figure 2. a) Representative HRTEM image showing the superstructure of CNH–H_2P nanohybrids, and b) particle size distribution of soluble CNH–H_2P nanohybrids as estimated by light-scattering measurements.

affect or alter the original dahlia-flower-like morphology of the CNH aggregates. In addition, the average diameter of the CNH–H_2P aggregates is estimated by DLS to be around 280 nm; aggregates with diameters as small as 85 nm are also observed in solution (Fig. 2b).

The oxidized CNHs show very good thermal stability below 509 °C under a nitrogen atmosphere, as revealed by thermogravimetric analysis (TGA). The grafting of H_2P onto the CNHs is corroborated by the degradation of the CNH–H_2P nanohybrids at this temperature. TGA reveals a 21.3 wt % decrease in weight for the nanohybrid sample at 509 °C, which corresponds to the amount of H_2P attached to the nanohorns (Fig. 3). However, at 509 °C, unbound H_2P constitutes 30 wt % of the porphyrin in the sample (Fig. 3); and thus, 14 wt % is the fraction of H_2P covalently attached to the nanohorns. The weight loss from 509 to 625 °C, with the major loss occurring at 575 °C, is attributed to the oxidized CNHs.

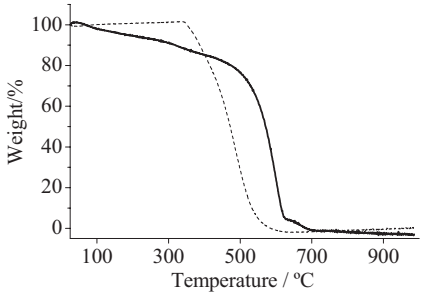

Figure 3. TGA curves of CNH–H_2P nanohybrids (solid line) and unbound H_2P (dotted line).

The first spectroscopic insight into the covalent attachment of H_2P to the CNHs comes from vibrational spectroscopy. In the attenuated total reflectance (ATR) IR spectrum of CNH–H_2P nanohybrids, the characteristic amide carbonyl peaks are observed at 1658 and 1635 cm^{-1}, whereas the carbonyl vibration due to the carboxylic units of the oxidized CNHs is seen at around 1745 cm^{-1} (Fig. 4). Moreover, the stretching and bending modes of aromatic C–H from the porphyrin skeleton are identified in the range between 2847 and 2965 cm^{-1}.

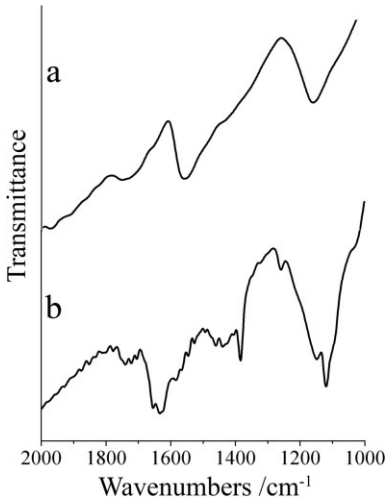

Figure 4. ATR-IR spectra of a) oxidized CNHs and b) CNH–H_2P nanohybrids.

Raman spectroscopy of the CNH–H_2P nanohybrids reveals the presence of two strong bands, the D- and G-bands that are almost equal in strength at 1270 and 1593 cm^{-1}, respectively. These bands are known to be characteristic of CNHs.[13] Figure 5 compares the Raman spectra (excitation wavelength of 1064 nm) of the as-grown CNHs, oxidized CNHs, and CNH–H_2P nanohybrids. The G-band at 1593 cm^{-1} is assigned to the E_{2g}-like vibrations of the sp^2-hybridized carbon network, whereas the D-band at 1270 cm^{-1} is associated with the A_{1g}-re-

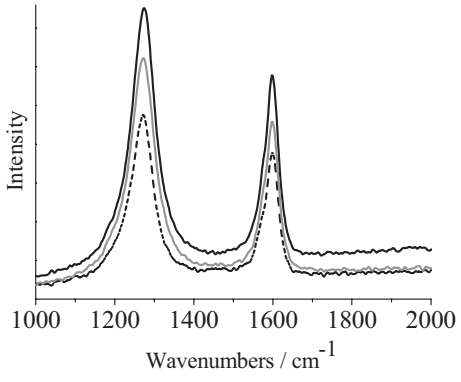

Figure 5. Raman spectra of as-grown CNHs (dotted line), oxidized CNHs (grey line), and CNH–H_2P nanohybrids (black line). The laser wavelength is 1064 nm and the laser power used is 360 mW.

lated modes derived from the loss of the basal plane lattice periodicity induced by the conical shape of the CNH tips.[14] It is apparent that the only significant change in the Raman spectra of the CNHs after the oxidation process is an increase in the intensity of the D-band due to the generation of defect sites. These defects arise from the introduction of carboxylic units during oxidation rather than the presence and/or generation of graphitic- and/or amorphous-like carbon material. Therefore, the increase in the intensity of the D-band for the CNH–H_2P nanohybrids as compared to that of the as-grown CNHs is attributed to the introduction of defects in the CNHs after the functionalization treatment and grafting of porphyrin units.[15]

Continuing the spectroscopic characterization of the CNH–H_2P nanohybrids with electronic absorption spectroscopy, the characteristic Soret band due to the porphyrin unit is identified at 420 and 523 nm, whereas the Q-bands of the porphyrin unit are observed at 523, 559, 586, and 617 nm; the presence of the CNHs is manifested by the continuous absorbance from the NIR to the UV-vis region of the electromagnetic spectrum (Fig. 6). Moreover, the Soret and Q-bands of the CNH–H_2P nanohybrids are broadened and red-shifted by approximately 3 nm, as compared to the corresponding bands of unbound H_2P, suggesting the occurrence of electronic communication between the porphyrin moieties and the nanohorns in the ground state.

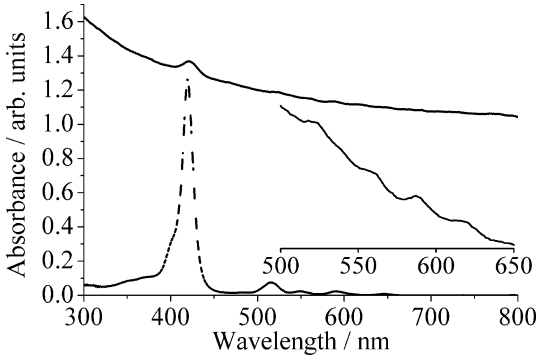

Figure 6. Electronic absorption spectra of unbound H_2P (dotted line) and CNH–H_2P nanohybrids (solid line). The spectra have been measured in dichloromethane using a cell with a 1 cm optical path. The inset shows an expanded view of the Q-band region of the CNH–H_2P nanohybrids.

Fluorescence spectroscopy is a useful tool for assessing the degree of electronic communication in the excited states of the CNH–H_2P nanohybrids. The strong fluorescence emission of photoexcited H_2P at 650 and 720 nm is significantly quenched in the covalently associated CNH–H_2P nanohybrids (Fig. 7), confirming that the H_2P moieties are in close proximity to the CNHs in the nanohybrids (enabling sufficient electronic communication between the two species).

The excited state dynamics of the CNH–H_2P nanohybrids has been elucidated by time-resolved spectroscopy studies. In this context, the emission–time profiles of the nanohybrids are characterized by quick decays, as compared to those for unbound H_2P (Fig. 8). Indeed, this is nicely consistent with the

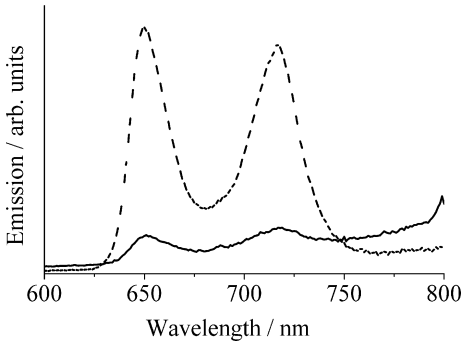

Figure 7. Fluorescence spectra of unbound H_2P (dotted line) and CNH–H_2P nanohybrids (solid line). The spectra have been measured in dichloromethane with λ_{ex} = 420 nm. The concentrations are adjusted so that the samples exhibit equal absorbance at the excitation wavelength.

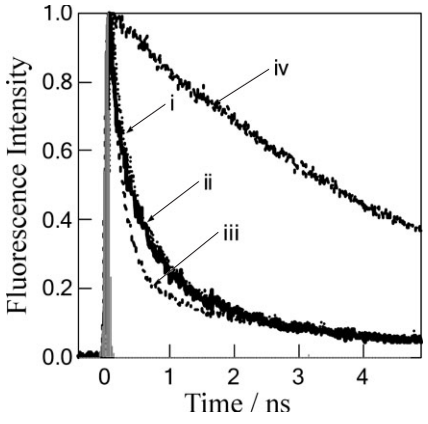

Figure 8. Fluorescence decay lifetimes of CNH–H_2P nanohybrids in i) toluene, ii) dichloromethane, and iii) benzonitrile. iv) Fluorescence decay lifetime of unbound H_2P in toluene. λ_{ex} = 400 nm.

observed steady-state fluorescence quenching. From the initial decay profiles, short fluorescence lifetimes, ranging from 240–260 ps, have been measured, as listed in Table 1. The decreased fluorescence lifetimes as compared to those measured for unbound H_2P (ca. 4900 ps) imply the rapid deactivation of photoexcited H_2P. Since the fluorescence lifetimes become shorter with increasing solvent polarity, it is reasonable to assume that charge separation occurs within the nanohybrid in polar sol-

Table 1. Fluorescence lifetimes (τ_f at 600–750 nm), charge-separation rate constants (k^S_{CS}), and quantum yields (Φ^S_{CS}) via $^1H_2P^*$. Charge-recombination rate constants (k_{CR}), lifetimes of the radical ion pair (τ_{RIP}), and yield of $HV^{\bullet+}$ ($\Phi_{HV^{\bullet+}}$) for CNH–H_2P nanohybrids.

Solvent	τ_f [ps]	k^S_{CS} [a] [s^{-1}]	Φ^S_{CS} [a]	k_{CR} [s^{-1}]	τ_{RIP} [ns]	$\Phi_{HV^{\bullet+}}$ [%]
$PhCH_3$	380	2.4×10^9 [b]	0.92 [b]	7.7×10^6 [c]	130 [c]	[d]
CH_2Cl_2	260	3.6×10^9	0.95	9.6×10^6	104	70
PhCN	240	4.0×10^9	0.95	1.8×10^7	56	85

[a] $k^S_{CS} = (1/\tau_f)_{sample} - (1/\tau_f)_{ref}$, $\Phi^S_{CS} = k^S_{CS}/(1/\tau_f)_{sample}$. [b] Energy transfer. [c] Triplet decay and triplet lifetime. [d] $HV^{2+}(PF_6^-)$ does not dissolve in toluene.

vents; more specifically, this means the oxidation of the porphyrin unit and reduction of the nanohorns, resulting in the formation of the charge-separated state $CNH^{\bullet-}$–$H_2P^{\bullet+}$. This result is in agreement with earlier work reporting photoinduced electron transfer between carbon nanotubes and free or metallated porphyrins attached to the nanotubes by covalent and supramolecular interactions.[10] Thus, the rate constants (k^S_{CS}) and quantum yields (Φ^S_{CS}) for charge separation via $^1H_2P^*$ can be determined, as listed in Table 1.

In non-polar solvents, these results suggest intramolecular photoinduced excited-state energy transfer, which is in accordance with recent reports on hybrid nanosystems formed between complexed or covalently linked porphyrins and carbon nanotubes.[11b,10k] Therefore, the quenching rate constants and quantum yields via $^1H_2P^*$ (Table 1) can be attributed to energy transfer.

Further support for this charge-separation scenario is obtained by comparing the total energy of singlet excited H_2P (1.90 eV) with that of the radical ion pair (RIP) state, $CNH^{\bullet-}$–$H_2P^{\bullet+}$. From cyclic voltammetry, the oxidation potential of H_2P is observed at 0.68 V versus $Ag/AgCl^+$, whereas the reduction potential of CNHs appears as a weak signal in benzonitrile at –0.04 V versus $Ag/AgCl^+$; the latter signal does not always imply the intrinsic reduction potential of the CNHs, but also reflects the defects introduced during sample preparation (Fig. S4, Supporting Information). The total energy of the RIP state calculated from these potentials is determined to be 0.72 eV in benzonitrile. Therefore, a value of –1.18 eV is derived as the free-energy change for photoinduced charge separation of the nanohybrid system via $^1H_2P^*$ in a polar solvent such as benzonitrile. The free-energy change tends to approach zero with decreasing polarity of the solvent.

In order to shed light and follow the formation of photoinduced charge-separated states within the CNH–H_2P nanohybrids, additional experiments have been conducted with the aid of an electron mediator, hexyl-viologen dication (HV^{2+}), and an electron–hole shifter, 1-benzyl-1,4-dihydronicotinamide (BNAH).[16] In this context, upon the addition of HV^{2+} and BNAH to the nanohybrid CNH–H_2P system in polar solvents, the accumulation of $HV^{\bullet+}$ is observed (Fig. 9) by repeated 532 nm laser excitation of the H_2P moiety. This observation indirectly supports the photoinduced generation of $CNH^{\bullet-}$–$H_2P^{\bullet+}$, which mediates electron transfer to HV^{2+}. Since the $HV^{\bullet+}$ concentration increases with increasing amounts of BNAH, the hole is transferred from $H_2P^{\bullet+}$ to BNAH, resulting in the formation of H_2P and $BNAH^{\bullet+}$; the latter is quickly transformed to the closed-shell 1-benzyl-nicotinamidinium ion (BNA^+) possessing a poor electron-accepting ability. Indeed, during the accumulation of $HV^{\bullet+}$, the absorbance of H_2P remains constant. From the maximum $HV^{\bullet+}$ concentration ($Abs(HV^{\bullet+})$) observed upon repeated 532 nm laser light excitation, the conversion of the added HV^{2+} to $HV^{\bullet+}$ is estimated to be 85 % in benzonitrile and 75 % in CH_2Cl_2. These conversion values are appreciably higher than that measured for tetracationic-porphyrin–CNH hybrids in aqueous solution (24 %) under the same experimental conditions. In a control experiment, negligible accumulation of $HV^{\bullet+}$ is observed upon the laser excitation of a benzonitrile solution of H_2P at 532 nm in the absence of CNHs using similar concentrations of H_2P, HV^{2+}, and BNAH (Fig. S5, Supporting Information). Thus, the CNHs are necessary for the accumulation of $HV^{\bullet+}$.

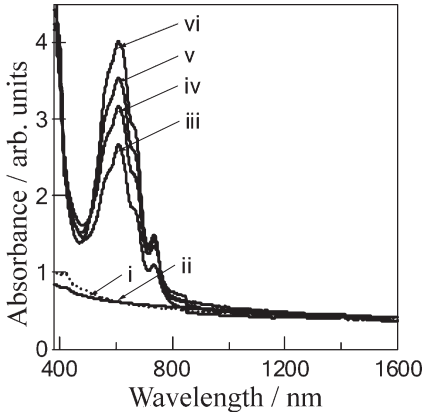

Figure 9. Changes in the steady-state absorption spectra of CNH–H_2P nanohybrids in the presence of 0.5 mM HV^{2+} and BNAH (the cell length is 0.5 cm) i) before and ii–vi) after repeated 532 nm laser light excitation (ca. 3 mJ $pulse^{-1}$). The BNAH concentrations are ii) 0 mM, iii) 0.5 mM, iv) 1.0 mM, v) 1.5 mM, and vi) 2.0 mM in deaerated benzonitrile.

Additional support for the above hypothesis comes from complementary transient absorption spectroscopy measurements performed after laser irradiation of the CNH–H_2P nanohybrids at 532 nm. Upon photoexciting the Q-band of H_2P at 532 nm with short laser pulses, it should be possible to identify the transient and/or derived products, and it should also be possible to resolve their decay rates. In the absence of oxygen, transient absorption bands are observed from the visible to the NIR region of the spectrum, as shown in Figure 10. The characteristic features of the triplet–triplet absorption of H_2P are missing in polar solvents (Figs. S6 and S7, Supporting Informa-

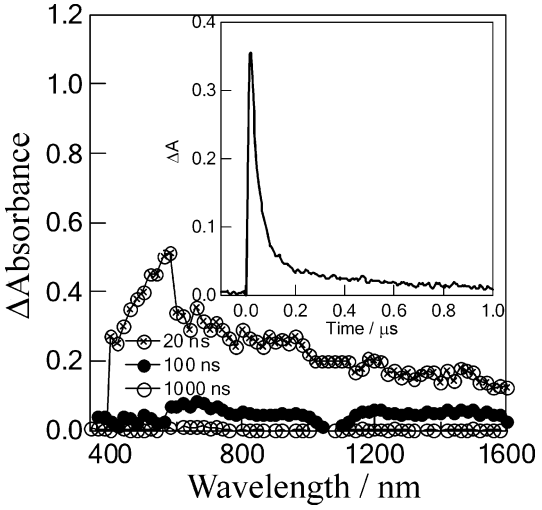

Figure 10. Nanosecond transient absorption spectra of CNH–H_2P nanohybrids (ca. 0.2 mg in 2 mL) obtained upon 532 nm (ca. 3 mJ $pulse^{-1}$) laser irradiation in benzonitrile (at 0.02 μs (⊗), 0.1 μs (●), and 1.0 μs (○)). The inset shows the absorption–time profiles at 660 nm.

tion), thus suggesting the efficient quenching of the singlet excited state by the CNHs. The absorption band observed in the visible region near 550 nm corresponds to the one-electron oxidized product, $H_2P^{\bullet+}$,[17] although peaks arising from the scattering of the 532 nm laser light by the dispersed particles are overlapped; a similar depletion is observed near 1100 nm due to the fundamental frequency of the yttrium aluminum garnet (YAG) laser. In addition, the broad bands in the NIR region can be ascribed to electrons trapped within the reduced nanohorns (i.e., $CNH^{\bullet-}$), similar to the situation identified in higher fullerene radical anions.[18] Thus, considering all the above observations, it is reasonable to postulate that the decay rates of the transient absorption bands can be attributed to charge recombination, which occurs after the formation of a charge-separated state in the $CNH^{\bullet-}$–$H_2P^{\bullet+}$ nanohybrids. From the decay time profiles of these transient bands, the rate constants of the charge recombination process are calculated to be 1.8×10^7 s^{-1} in benzonitrile and 9.6×10^6 s^{-1} in dichloromethane, which corresponds to 60 and 100 ns lifetimes for $CNH^{\bullet-}$–$H_2P^{\bullet+}$, respectively, in the two solvents. The decay of the RIP results in the recovery of the ground state of the CNH–H_2P nanohybrid since population of the triplet excited state of H_2P is thermodynamically unfavorable. This is because the charge-separated state is far lower in energy than the energy level of triplet excited H_2P.[19]

Upon the addition of HV^{2+} and BNAH, most of the transient bands disappear, leaving only the 620 nm band of $HV^{\bullet+}$, as shown in Figure 11. This supports the conclusion that the transient absorption bands in Figure 8 are overlapped bands of $CNH^{\bullet-}$–$H_2P^{\bullet+}$. From the rapid increase in concentration of $HV^{\bullet+}$, corresponding to the quick decay of $CNH^{\bullet-}$–$H_2P^{\bullet+}$ in the presence of HV^{2+}, the intermolecular electron migration rate is evaluated to be 5.0×10^9 M^{-1} s^{-1}, which is close to the diffusion controlled limit. The slow increase in the concentration of HV^+ may correspond to intermolecular electron transfer from the excited state of H_2P to HV^{2+}.

On the other hand, in non-polar toluene, it is difficult to confirm charge separation using HV^{2+} and BNAH due to the low solubility of these molecules. However, the triplet–triplet absorption band is clearly observed in the transient spectra, suggesting that charge separation likely does not occur. As a result, the observed efficient fluorescence quenching can be attributed to energy transfer.

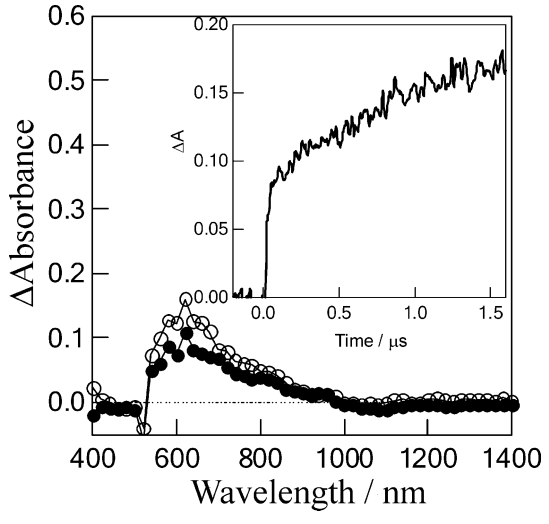

Figure 11. Nanosecond transient absorption spectra of CNH–H_2P nanohybrids (ca. 0.2 mg in 2 mL) in the presence of 3 mM HV^{2+} and 3 mM BNAH obtained upon 532 nm (ca. 3 mJ $pulse^{-1}$) laser irradiation in benzonitrile (at 0.1 μs (●) and 1.0 μs (○)). The inset shows the absorption–time profile at 620 nm.

3. Conclusions

Oxidized CNHs have been covalently functionalized with H_2P, resulting in the formation of CNH–H_2P nanohybrids. These nanohybrids have been characterized by optical spectroscopy and electron microscopy. The CNH–H_2P nanohybrids form a stable ink-like solution while still retaining the original aggregated superstructure of the CNHs. Fluorescence quenching on the 240–260 ps time scale and nanosecond transient absorption spectroscopy results indicate that the CNHs serve as electron acceptors and the photoexcited H_2P moieties serve as electron donors, resulting in the formation of a charge-separated state $CNH^{\bullet-}$–$H_2P^{\bullet+}$ in polar solvents. In non-polar solvents, the intramolecular energy-transfer quenching of the photoexcited H_2P singlet excited state by CNHs is shown to occur on a 380 ps time scale.

Having developed suitable functionalization methods for the covalent grafting of organic units onto CNHs, we are currently working towards the synthesis of more advanced CNH-based hybrid materials incorporating additional photo- and/or electroactive components (such as metallocenes and tetrathiafulvalenes).

4. Experimental

General Information: ^1H (500 MHz, 300 MHz) and ^{13}C (125 MHz, 75 MHz) NMR spectra were recorded on Bruker Avance spectrometers and referenced to the residual protonated solvent. Mass spectra were measured on a MS/MS ZABSpec time-of-flight (TOF) spectrometer at the University of Rennes I (CRMPO). Steady-state UV-vis electronic absorption spectra were recorded on Varian Cary 1E, Uvikon XL, and Perkin Elmer (Lambda 19) UV-vis-NIR spectrophotometers. IR spectra were recorded on Bruker IFS 66 and 28 spectrometers. Solvents (American Chemical Society (ACS) grade for analysis) were purchased from Aldrich and Carlo Erba. THF was distilled from potassium metal, whereas methanol was distilled from magnesium turnings. Dichloromethane was used as received. Triethylamine was distilled from CaH_2. The starting materials were generally used as received (Acros, Aldrich) without any further purification, unless otherwise stated. All reactions were performed under an argon atmosphere and monitored by thin-layer chromatography (TLC) (silica, CH_2Cl_2/MeOH). Column flash chromatography was performed on a silica gel column (Merck TLC-Kieselgel 60H, 15 μm). Elemental analysis data was obtained on an EA 1108 Fisons instrument. Steady-state emission spectra were recorded on a Fluorolog-3 Jobin Yvon-Spex spectrofluorometer (model GL3-21). The picosecond time-resolved fluorescence spectra were measured using a Ti:sapphire laser (Tsunami) and a streak scope (Hamamatsu Photonics). Nanosecond transient absorption spectra in the visible and NIR regions were measured by laser flash photol-

ADVANCED FUNCTIONAL MATERIALS

ysis; 532 nm light from a Nd:YAG laser was used as the excitation source and Si- and Ge-avalanche-photodiode modules were used for detecting the monitoring light from a pulsed Xe lamp, as described in our previous reports [20]. All experiments were performed at room temperature.

Received: January 9, 2007
Revised: February 13, 2007
Published online: May 30, 2007

[1] a) *Introduction to Nanotechnology* (Eds: C. P. Poole, F. J. Owens), Wiley-VCH, Weinheim **2003**. b) *Nanophysics and Nanotechnology: An Introduction to Modern Concepts in Nanoscience* (Ed: E. L. Wolf), Wiley, New York **2004**.

[2] a) S. Iijima, M. Yudasaka, R. Yamada, S. Bandow, K. Suenega, F. Kokai, K. Takahashi, *Chem. Phys. Lett.* **1999**, *309*, 165. b) S. Iijima, *Physica B* **2002**, *323*, 1.

[3] a) T. Ohba, K. Murata, K. Kaneko, W. A. Steele, F. Kokai, K. Takahashi, D. Kasuya, M. Yudasaka, S. Iijima, *Nano Lett.* **2001**, *1*, 371. b) K. Murata, A. Hashimoto, M. Yudasaka, D. Kasuya, K. Kaneko, S. Iijima, *Adv. Mater.* **2004**, *16*, 1520. c) H. Tanaka, H. Kanoh, M. Yudasaka, S. Iijima, K. Kaneko, *J. Am. Chem. Soc.* **2005**, *127*, 1217. d) S. Utsumi, K. Urita, H. Kanoh, M. Yudasaka, K. Suenaga, S. Iijima, K. Kaneno, *J. Phys. Chem. B* **2006**, *110*, 7165.

[4] a) A. Hashimoto, H. Yorimitsu, K. Azima, K. Suenaga, H. Isobe, A. Miyawaki, M. Yudasaka, S. Iijima, E. Nakamura, *Proc. Natl. Acad. Sci. USA* **2004**, *101*, 8527. b) T. Murakami, K. Ajima, J. Miyawaki, M. Yudasaka, S. Ijima, S. Shiba, *Mol. Pharmacol.* **2004**, *1*, 399. c) K. Ajima, M. Yudasaka, T. Murakami, A. Maigne, K. Shiba, S. Iijima, *Mol. Pharmacol.* **2005**, *2*, 475. d) M. Zhang, M. Yudasaka, J. Miyawaki, J. Fan, S. Ijima, *J. Phys. Chem. B* **2005**, *109*, 22 201.

[5] a) N. Tagmatarchis, A. Maigne, M. Yudasaka, S. Iijima, *Small* **2006**, *2*, 490. b) C. Cioffi, S. Campidelli, F. G. Brunetti, M. Meneghetti, M. Prato, *Chem. Commun.* **2006**, 2129.

[6] G. Pagona, N. Tagmatarchis, J. Fan, M. Yudasaka, S. Iijima, *Chem. Mater.* **2006**, *18*, 3918.

[7] I. D. Petsalakis, G. Pagona, G. Theodorakopoulos, N. Tagmatarchis, M. Yudasaka, S. Iijima, *Chem. Phys. Lett.* **2006**, *429*, 194.

[8] J. Zhu, M. Yudasaka, M. Zhang, D. Kasuya, S. Iijima, *Nano Lett.* **2003**, *3*, 1239.

[9] G. Pagona, A. S. D. Sandanayaka, Y. Araki, J. Fan, N. Tagmatarchis, M. Yudasaka, S. Iijima, O. Ito, *J. Phys. Chem. B* **2006**, *110*, 20 729.

[10] a) H. Murakami, T. Nomura, N. Nakashima, *Chem. Phys. Lett.* **2003**, *378*, 481. b) H. Li, B. Zhou, Y. Lin, L. Gu, W. Wang, K. A. S. Fernando, K. Kumar, L. F. Allard, Y.-P. Sun, *J. Am. Chem. Soc.* **2004**, *126*, 1014. c) D. M. Guldi, G. M. A. Rahman, N. Jux, N. Tagmatarchis, M. Prato, *Angew. Chem. Int. Ed.* **2004**, *43*, 5526. d) T. Hasobe, S. Fukuzumi, P. V. Kamat, *J. Am. Chem. Soc.* **2005**, *127*, 11 884. e) A. Satake, Y. Miyajima, Y. Kobuke, *Chem. Mater.* **2005**, *17*, 716. f) J. Chen, C. P. Vollier, *J. Phys. Chem. B* **2005**, *109*, 7605. g) F. Cheng, S. Zhang, A. Adronov, L. Echegoyen, F. Diederich, *Chem. Eur. J.* **2006**, *12*, 6062. h) D. M. Guldi, G. M. A. Rahman, S. Qin, M. Tchoul, W. T. Ford, M. Marcaccio, D. Paolucci, F. Paolucci, S. Campidelli, M. Prato, *Chem. Eur. J.* **2006**, *12*, 2152. i) F. Y. Chen, A. Adronov, *Chem. Eur. J.* **2006**, *12*, 5053. j) H. Tanaka, T. Yajima, T. Matsumoto, Y. Otsuka, T. Ogawa, *Adv. Mater.* **2006**, *18*, 1411. k) M. Alvaro, P. Atienzar, P. de la Cruz, J. L. Delgado, V. Troiani, H. Garcia, F. Langa, A. Palkar, L. Echegoyen, *J. Am. Chem. Soc.* **2006**, *128*, 6626.

[11] a) Z. Guo, F. Du, D. Ren, Y. Chen, J. Zheng, Z. Liu, J. Tian, *J. Mater. Chem.* **2006**, *16*, 3021. b) D. Baskaran, J. W. Mays, X. P. Zhang, M. S. Bratcher, *J. Am. Chem. Soc.* **2005**, *127*, 6916. c) H. Li, R. B. Martin, B. A. Harruff, R. A. Carino, Y.-P. Sun, *Adv. Mater.* **2004**, *16*, 896.

[12] Z. Halime, M. Lachkar, N. Matsouki, G. Charalambidis, M. di Vaira, A. G. Coutsolelos, B. Boitrel, *Tetrahedron* **2006**, *62*, 3056.

[13] T. Yamaguchi, S. Bandow, S. Iijima, *Chem. Phys. Lett.* **2004**, *389*, 181.

[14] a) A. M. Rao, E. Richter, S. Bandow, B. Chase, P. C. Eklund, K. A. Williams, S. Fang, K. R. Subbaswamy, M. Menon, A. Thess, R. E. Smalley, G. Dresselhaus, M. S. Dresselhaus, *Science* **1997**, *275*, 187. b) S. Iijima, T. Ichihashi, Y. Ando, *Nature* **1992**, *356*, 776. c) F. Tuinstra, J. L. Koenig, *J. Compos. Mater.* **1970**, *4*, 492.

[15] C.-M. Yang, D. Kasuya, M. Yudasaka, M. Iijima, K. Kaneko, *J. Phys. Chem. B* **2004**, *108*, 17 775.

[16] S. Fukuzumi, T. Suenobu, M. Patz, T. Hirasaka, S. Itoh, M. Fujitsuka, O. Ito, *J. Am. Chem. Soc.* **1998**, *120*, 8060.

[17] J. Rodriguez, C. Kirmaier, D. Holten, *J. Am. Chem. Soc.* **1989**, *111*, 6500.

[18] M. Fujitsuka, O. Ito, in *Encyclopedia of Nanoscience and Nanotechnology* (Ed: H. S. Nalwa), American Scientific, Stevenson Ranch, CA **2004**, pp. 593-615.

[19] a) D. Kuciauskas, S. Lin, G. R. Seely, A. L. Moore, T. A. Moore, D. Gust, T. Drovetskaya, C. A. Reed, P. D. W. Boyd, *J. Phys. Chem.* **1996**, *100*, 15 926. b) H. Imahori, K. Tamaki, D. M. Guldi, C. Luo, M. Fujitsuka, O. Ito, Y. Sakata, S. Fukuzumi, *J. Am. Chem. Soc.* **2001**, *123*, 2607.

[20] a) A. S. D. Sandanayaka, K. Ikeshita, Y. Araki, N. Kihara, Y. Furusho, T. Takata, O. Ito, *J. Mater. Chem.* **2005**, *15*, 2276. b) G. A. Rajkumar, A. S. D. Sandanayaka, K. Ikeshita, Y. Araki, Y. Furusho, T. Takata, O. Ito, *J. Phys. Chem. B* **2006**, *110*, 6516.

